Characterization of physiological noise in resting-state fMRI data at 7T

Sandro Daniel Sabudin Nunes [a*]

[a] *Dept. Bioengineering, IST, Lisbon, Portugal*
** sandro.nunes@tecnico.ulisboa.pt*

A B S T R A C T

An increasing interest exists in the scientific community in studying functional brain networks measured by resting-state fMRI (rs-fMRI). The development of new fMRI acquisition techniques at ultra-high-field (7 Tesla), that allow full brain coverage with high sensitivity and spatial resolution, promises to provide significant insights into functional brain networks. Because measuring functional brain connectivity is based on the detection of synchronous neuronal activity between different regions, non-neuronal mechanisms producing correlated signal fluctuations will be reflected on the connectivity measurements. The characterization and removal of these spurious sources, most often referred to as physiological noise, has therefore become a major subject of concern, especially when going to ultra-high-field strengths where their contribution is significantly increased. This work aims to quantitatively characterize the correlated, physiological noise fluctuations in whole-brain, 1 mm^3-resolution rs-fMRI data collected from a group of healthy participants at 7 Tesla, both at a whole-brain level and at a more specific, region-based, tier. To that end, a nested-model general linear modeling (GLM) optimization approach was employed, which combines and compares a number of different well-established and promising techniques to model the main sources of physiological noise in the rs-fMRI signal. The optimal model that was found explained a total of 33.8%±5.9 SE of variance in gray matter, with the main source of signal fluctuations being explained by low-frequency drifts (19.6±3.3%), followed by cardiac and respiratory mechanisms (6.6±1.2 %), voxel displacements caused by motion (5.9±1.2%), and global fluctuations in the cerebrospinal fluid and white matter (1.3±0.2%). Correction techniques based on external physiological acquisitions proved to be invaluable as only 17.6±1.9% of spurious signal variance introduced by cardiac and respiratory mechanisms is expected to be alternatively removed by using data-based techniques alone. Subtle voxel displacements (5.0±0.8%), rather than large, abrupt movement (0.9±0.4%) were found to introduce the majority of motion-induced artefacts in the signal. Improvements in intrinsically problematic regions such as the brainstem were more modest, however the model still identified 25.8% putatively attributed to nuisance sources. In conclusion, we compared different methods for modelling correlated, physiological noise fluctuations in rs-fMRI data collected at 7 Tesla, and propose an optimal methodology that explains maximum signal variance. Future work will investigate the effects of the improved physiological noise correction on the identification and analysis of resting-state networks.

Keywords: Functional magnetic resonance imaging (fMRI); resting-state networks; functional brain connectivity; physiological noise modelling; RETROICOR; 7 Tesla

The fMRI technique has been continually improved in the last two decades in terms of image quality, spatial and temporal resolution, and sensitivity, mainly due to the employment of higher field strengths, (Wald et al., 2012). However, sensitivity in fMRI depends on multiple sources of variance, such as instrumental – thermal noise and electronic instabilities – and subject-dependent modulations associated with physiological processes (Triantafyllou et al., 2005). While thermal noise has a linear relation with the field strength, physiological noise grows higher than linearly, hampering the potential benefits of imaging with higher strength fields when not accounted for (Kruger et al., 2001). The need to model and regress out confounds with a physiological nature in fMRI data is, thus, apparent.

In resting-state fMRI (rs-fMRI), physiological noise is particularly relevant. Brain connectivity studies using resting-state fMRI acquisitions operate by measuring the common variance of the fMRI blood oxygenation level dependent (BOLD) signals in different brain regions to identify synchronous activity (Birn et al., 2013). Since these fluctuations are measured simultaneously, any non-neuronal activity-related process that affects either time series will yield a spurious result. Supported by the recent and ongoing popularity of resting-state imaging, much effort has been put into new noise removal techniques, allowing more subtle measures to be made and increasing the confidence in the information extracted. However, complete understanding of the causal relation between physiological manifestations and functional connectivity is far from being reached. There is still no ground truth nor an absolute optimal model that suits every analysis, making the task of choosing the most appropriate set of techniques to employ in each situation not a trivial one. This problem keeps driving the scientific community towards improving the knowledge on the sources of physiological noise plaguing hampering fMRI data and the tools used to remove them.

1.1. Sources of physiological noise

A very significant fraction of the spurious fluctuations introduced in the data are caused by cardiac and respiratory mechanisms. Both Cardiac and respiratory cycles introduce fluctuations in the measured fMRI signal by inducing changes in the cerebral blood flow (CBF), cerebral blood volume (CBV) and arterial pulsatility (Greitz et al., 1993; Purdon et al., 1998; Dagli et al., 1999; Kruger et al., 2001) or through changes in the static magnetic field (Raj et al., 2011) and arterial CO_2 partial pressure (Wise et al., 2004). Additionally, interaction effects such as an increased cardiac output during inspiration (the “respiratory pump”, Hayen et al., 2013) may also have a manifest impact on the MRI signal. Some changes are due to real movements, such as pulsatility and respiratory cyclic movements (Dagli et al., 1999), while others cause apparent movement by geometric distortion, as with changing B_0 fields induced by the variable air volume in the thorax (Raj et al., 2011).

Correlations between changes in cardiac and respiratory rates and BOLD signal have also been demonstrated to be significant sources of confound (Birn et al., 2006; Shmueli et al., 2007; Wise et al., 2004). Fluctuations caused by these mechanisms are within the frequency range of resting-state BOLD oscillations, arising from changes in arterial CO_2 concentration and blood pressure.

Cerebrospinal fluid pulsation causes voxel displacement and brain distortion due to induced movements in subcortical structures and introduces spurious temporal correlations due to the flow of unsaturated CSF spins into the imaging slice (Brooks et al., 2013). Motion is also an important source of spurious fluctuations, not only due to voxel displacements caused by head motion, but also because it modifies the uniformity of the magnetic field and changes the steady state magnetization by changing the time between excitations in parts of the tissue that changed position (spin history effects). Changes in signal intensity due to spin history effects produce significant changes in the BOLD signal (up to twice the expected BOLD signal, Muresan et al., 2005) and are not corrected by standard pre-processing methods.

1.2. Correcting physiological noise in resting-state fMRI data

Many different approaches have been suggested over the last years to deal with physiological noise. These methods can be subdivided into three major fields: data acquisition techniques, pre-processing strategies and physiological modelling.

Acquisition-based strategies tackle this issue in a number of ways: capturing images at a fixed point in the physiological process that is generating noise (Malinen et al., 2006); minimizing the presence of physiologically-induced image artefacts by optimizing sequence parameters (Pfeuffer et al., 2001); acquiring additional scans to help identify physiological noise sources from an independent acquisition (calibration scans, de Zwart et al., 2008).

Pre-processing techniques may range from simply filtering out the frequencies associated with cardiac and respiratory mechanisms, which is not generally advisable due to the aliasing of these frequencies to the lower end of the spectrum, to more sophisticated methods. RETROKCOR (Hu et al., 1995) operates on the k-space by regressing out signals related to the timing of the cardiac and respiratory cycles using externally acquired signals. Independent component analysis (ICA) has also been shown to be capable of separating instrumentation artefacts, physiological sources and neuronal-induced fluctuations (Beckmann et al., 2004; Smith et al., 2013), however results still heavily rely on matching between the training data and the acquisition being analyzed (Churchill et al., 2012).

Modelling is currently the most common approach to account for physiological noise. These techniques can be placed into two major categories: a) techniques that estimate physiological contributions directly from the data; b) techniques that use external physiological recordings to obtain confounds. Their use is not mutually exclusive and they are often used simultaneously. Data-based techniques to handle motion artifacts are not exclusive of connectivity studies and are commonly used to remove motion artifacts which could not be removed during motion correction in the pre-processing stage. These techniques attempt to remove spin history effects by regressing out the six rigid body parameters (Friston et al., 1996; Jenkinson et al., 2002) and by "scrubbing" the data, which consists in detecting excessive motion volumes and excluding them from functional analysis. (Power et al. 2012; Satterthwaite et al., 2013, Carp et al. 2013). Regressing out white matter (WM) and cerebrospinal fluid (CSF) average time-courses is also a common procedure and works on the assumption that signal coming from these regions is unlikely to show neuronal activity-induced BOLD fluctuations (Birn et al., 2009; Weissenbacher et al., 2009; Jo Hang et al., 2011). In the other hand, techniques such as the Retrospective Image Correction (RETROICOR) (Glover et al., 2000), a modification of the methodology proposed by Hu et al.,1995 that operates at the image space, attempt to model cardiac and respiratory quasi-periodic effects based on external physiological acquisitions. Recently, modeling lower frequency non-periodic fluctuations arising from cardiac and respiratory from the externally acquired data has also become more common. The respiratory volume per time (RVT) (Birn et al., 2009), which uses information regarding the timings and amplitude of the respiratory peaks to model the respiratory non-periodic fluctuations and the heart rate (HR) (Shmueli et al., 2007) both have been reported to explain an additional spurious fraction of the BOLD signal.

In this study, both data and physiological recordings based techniques will be reviewed and implemented under the framework of the GLM. An exhaustive comparison between well-established approaches and promising state-of-the-art techniques on physiological noise modelling is provided both at a whole brain level and at a specific, ROI-based, tier. While not prescriptive, this methodology intends to provide accurate guidelines on the adequate physiological model to employ when processing resting-state functional connectivity data acquired at high field strengths.

2. Materials and Methods

The data were acquired on a 7 T Siemens whole-body scanner equipped with a custom-built 32-channel receive birdcage RF coil, at the Athinoula A. Martinos Center for Biomedical Imaging, in the scope of the FCT funded project HiFi-MRI: Whole-Brain Functional Connectivity Analysis of Ultra High Field MRI. Twelve healthy volunteers underwent an rs-fMRI scan and a structural imaging scan, while both cardiac and respiratory data were simultaneously recorded.

2.1. Data acquisition

Data were acquired from 12 healthy subjects by means of a simultaneous Multi-Slice (SMS) EPI sequence performed on a 7 T Siemens whole-body scanner equipped with a custom-built 32-channel receiving birdcage coil. A whole brain 1.1 mm isotropic scan covering 123 sagittal slices was acquired from each subject with TE=32 ms, TR=2500 ms, flip angle = 75º, FOV=264x198 mm^2. Slices were acquired in an interleaved order with a GRAPPA acceleration factor of 3. Whole-brain T1-weighted structural images using a MPRAGE sequence were also obtained during the scanning session. Subjects' cardiac data was recorded using a pulse transducer (TN1012/ST, ADInstruments) placed on the left index finger. Respiratory data was measured with a pneumatic belt (UFI Model 1132 Pneumotrace II, UFI) strapped around the subjects' upper abdomen. Both cardiac and respiratory traces, along with a trace signaling the MRI scan triggers, were acquired with a sampling rate of 1000 Hz.

2.2. Data pre-processing

In order to extract the phase of the cardiac cycle required to compute some of the regressors used in the model, cardiac peaks were identified on a low-pass filtered (f_c=1.6 Hz) version of the cardiac trace. No peak detection was carried out on the respiratory signal, however low-pass filtering was still applied (f_c=1.1 Hz) to remove spurious, non-respiratory, fluctuations.

Data were pre-processed in FSL (Jenkinson et al., 2012; Smith et al. 2004). The fMRI data was firstly motion and slice-timing corrected. Non-brain structures were removed and spatial smoothing with a FWHM=1.5 mm kernel was applied to the data. Instead of applying a high-pass to remove low-frequency drifts in the data, these were later accounted for during regression in the GLM by means of a set of polynomial regressors up to the 3rd order. Additionally, to account for discontinuities in 3 of the datasets introduced by an RF instability, a procedure similar to motion outlier removal was used: an all zeros regressors except for a value of one at the time point correspondent to the discontinuity volume was added to the design matrix, fully modeling the influence of that time point with no adverse effects on the statistics. Images were finally registered to the MNI space by non-linear registration. Subjects 7 and 10 datasets were discarded due to heavy artefacts in the data, while subject 2 dataset was discarded due to a corrupted cardiac acquisition, yielding a final sample of 9 subjects.

2.3. Model optimization and performance evaluation

The model comparison procedure used in this study is based on Bianciardi et al. (2009). This methodology encompasses the successive addition of each set of regressors to the model, followed by a performance test to determine whether or not it should be included. This generates a succession of nested models with different levels of complexity. In order to account for differences in the number of degrees of freedom (DOF) and allow direct comparison between models with different levels of complexity, R^2_{adj} was employed:

$$\boldsymbol{R^2_{adj} = 1 - \frac{N-1}{N-P-1}\frac{\sum_{i=1}^{N}(y_i - y_i')^2}{\sum_{i=1}^{N}(y-\bar{y})^2}} \qquad (1)$$

where N is the number of volumes in the dataset, P is the number of regressors in the design matrix, y_i and y_i' are respectively the i-th value of y (the fMRI data), and y' (the approximation of y computed by the model) and $\bar{y}$ is the temporal mean of y.

The variance explained (VE) by a given regressor subset (X_n) was defined as in Bianciardi et al., 2009. Given a subset X_n, $VE(X_n)$ is given by:

$$VE(X_n) = (R^2_{adj}(DM_N) - R^2_{adj}(DM_{N-1})) \times 100 \qquad (2)$$

where $DM_N = [X_1\ X_2 \dots X_{N-1}\ X_N]$ and $DM_{N-1} = [X_1\ X_2 \dots X_{N-1}]$ are the design matrixes corresponding to nested models differing only in X_n.

2.4. Regressors extraction

The methodology followed to extract the various regressors tested is briefly described in this section.

Slow drifts

Low-frequency drifts in the data were accounted for by fitting up to the 3rd order polynomials. This method was chosen, rather than high-pass filtering, since it avoids time-series truncation effects on the Fourier spectrum and allows the quantification of the VE by these fluctuations.

RETROICOR

The RETROICOR technique proposed by Glover et al. (2000) models quasi-periodic cardiac and respiratory fluctuations by fitting the cardiac and respiratory cycles phase to a low-order Fourier series. The cardiac phase is defined as:

$$\boldsymbol{\varphi_c(t) = 2\pi\frac{t - t_1}{t_2 - t_1}} \qquad (3)$$

where t_1 and t_2 are the times of the R-wave peaks in the cardiac cycle respectively preceding and succeeding t, previously extracted from the cardiac trace.

The respiratory phase is defined as:

$$\boldsymbol{\varphi_r(t) = sign\left(\frac{dx}{dt}(t)\right)\pi\frac{\sum_{b=1}^{round(100x(t)/x_{max})}H(b)}{\sum_{b=1}^{100}H(b)}} \qquad (4)$$

where $H(b)$ is a 100 bin histogram of the respiratory amplitude signal x(t). The amplitude of the signal is accounted for by generating a histogram-equalized transfer function between the respiratory amplitude and $\varphi_r(t)$, where end-expiration is assigned a phase of zero and peak inspiration is assigned a phase of $\pm\pi$. The term $sign(dx/dt\,(t))$ differentiates inspiration ($sign(dx/dt\,(t)) > 0$) from expiration ($sign(dx/dt\,(t)) < 0$).

In this study, an extended version of the RETROICOR, including higher orders of the Fourier series (the original proposition used orders up to the 2nd) and addition terms that reflect the interaction between the cardiac and respiratory cycles is tested. The interactions terms were defined as in Birn et al., (2008):

$$\boldsymbol{y_{int}(t) = \sum_{m_c=1}^{M_c}\sum_{m_r=1}^{M_r}(\beta_{1,m_c,m_r}\cos(m_c\varphi_c(t) \pm m_r\varphi_r(t)) + \beta_{2,m_c,m_r}\sin(m_c\varphi_c(t) \pm m_r\varphi_r(t)))} \qquad (5)$$

where $y_{int}(t)$ is the estimated interaction physiological contribution at time point t, $\varphi_n(t)$ refers to the computed phase and m_n is the order of the model ($m_n > 1$ corresponds to harmonics of the fundamental frequency). $\boldsymbol{\beta_{1,m_c,m_r}}$ and $\boldsymbol{\beta_{2,m_c,m_r}}$ denote the GLM parameters estimates.

Cardiac and respiratory regressors were generated up to the 4th order (16 regressors), while interaction regressors were generated up to the 2nd (32 regressors). A hierarchical comparison methodology based on the work by Harvey et al. (2008) (Fig. 1) was then carried out in other to determine the optimal set of cardiac respiratory and interaction orders.

Figure 1 - Nested model hierarchy used to optimize the RETROICOR respiratory and cardiac orders. Variance explained for each isolated set was computed from the differential R^2_{adj} between the models indicated. To simplify notation, only the number corresponding to the highest order of both cardiac (C) and respiratory (R) is used to define the model, although it should be noted that all lower orders and polynomial functions were included as well. An analogous approach was used to optimize the interaction terms.

RVT and HR

RVT was computed following the method proposed by Chang et al., (2009), which estimates the value of the respiratory volume by computing the standard deviation of the respiratory waveform in a 5 seconds sliding window (corresponding to 2 TRs) centered at each time point. Additionally, to account for outliers, values which were more than 1.96 standard deviations away from the median were replaced by spline interpolation (Bianciardi et al., 2009). Finally, the signal was low-pass filtered ($f_c = 0.3\ Hz$) to obtain a smoother trace.

HR was computed as in Shmueli et al., (2007):

$$\boldsymbol{HR(t_n) = \frac{1}{t_{n+1} - t_n}} \qquad (6)$$

where t_n are the time points corresponding to maximum peaks.

The signal was the subject to removal of spurious time points (by linear interpolation of the time points more than 1.96 standard deviations away from the median). A Gaussian filter with standard deviation $\sigma = 1$ was then applied to smooth the data, followed by interpolation to match the middle time point of each fMRI volume.

An optimization process was carried out in which different alternative models were tested: a) a model comprising the RVT and HR described above; b) a model in which these were convolved with the respiratory (RRF, Birn et al., 2009) and cardiac (CRF, Chang et al., 2009a) response functions; c) a model in which an optimized lagged version of these regressors was used after shifting each regressor over t ∈ [−20 20] s in 1s steps and determining the one that explained the most variance (optimization by temporal shifting was carried out both at a group and at a subject level); a double-lag approach in which 2 HR and 2 RVT optimal lags were used to model the biphasic behavior suggested by the impulse response functions proposed by Birn and Chang et al. The 14 resultants models (7 for HR and 7 for RVT) were compared by means of a 3-way repeated measures ANOVA. Main effects of the variable measured (RVT vs HR), lag specificity (group optimal lags vs subject specific optimal lags) and model type (single peak vs convolution with IRF vs double-lag) as well as interactions between effects were evaluated. Pairwise comparisons were performed through a post-hoc analysis on the analysis of variance.

CSF and WM average time courses

Five different methods were used to obtain a CSF mask from which the CSF regressor was extracted: a) a temporal variance mask was obtained from the pre-processed data and thresholded such that only the voxels whose variance lays in the top 20th percentile remain; this mask was then applied to the fMRI data to extract the mean time course for the voxels exhibiting the largest variance (Kong et al., 2012); b) a CSF mask was obtained from segmentation of each subject's structural data (the CSF partial volume estimate map was thresholded to 0.98) and registered to the functional space; erosion using a spherical kernel with 1.1 mm radius was used to improve mask specificity and avoid partial volume effects (PVE) with gray matter (GM) c) the segmented mask was split into two masks with distinct levels of specificity: a draining vessels mask (c1), which includes blood vessels and sulcal CSF and a large ventricles mask (c2), which is restricted to the right/left lateral, 3rd and 4th ventricles. PVE are expected to be much less frequent in the latter since the ventricles are relatively well defined and easily segmented (Jo, Hang et al., 2010); d) a fifth mask was obtained by defining a 3 mm^3 sphere within the right lateral ventricle with center coordinate at (19, -33, 18) in the MNI space and then registering it to each subjects functional space (Chang et al., 2009b). Each mask was finally applied to the fMRI data to extract the correspondent CSF time course. To differentiate the CSF time courses extracted from the masks defined in a), b), c1), c2) and d), these will be respectively referred to as $X_{HV\ CSF}$, $X_{SEG\ CSF}$, $X_{DV\ CSF}$ $X_{LV\ CSF}$ and $X_{RLV\ CSF}$.

The white matter mask was obtained by thresholding at 0.9 the respective partial volume map obtained through FAST segmentation in each subject's structural space and then eroded using a 4.5 mm^3 cubic kernel. Registration to functional space was done and the mask applied to the fMRI data to extract the white matter voxels contributing to the average time course. A pre-erosion mask will also be used for comparison purposes. Pre- and post-erosion WM time courses will be referred to as X_{WM} and $X_{WM\ erod}$.

Motion

To minimize motion-induced signal contributions, translations and rotations estimates computed by MCFLIRT for each acquired volume were added to the model. Additionally, volumes affected by large, abrupt, motion were identified and regressed out using a double-criteria procedure. Corrupted volumes were identified using both DVARS (D referring to temporal derivative of time courses, VAR referring to RMS variance over voxels, Power et al., 2012), which indexes the rate of change of BOLD signal across the entire brain at each time point and FD (framewise displacement), which expresses instantaneous head motion as a scalar quantity by condensing the information contained in the 6 motion parameters time series. A box-plot cutoff defined as the 75 percentile plus 1.5 of the interquartile range (75P + 1.5 IQR) was used as the peak threshold. For each outlier, an individual binary regressor was created to guarantee independence between parameter estimates (Lemieux et al., 2007).

2.5. ROI definition

To characterize the effect of these physiological sources in specific brain regions, different regions of interest (ROIs) were defined. Firstly, a gray matter mask was defined to evaluate the model performance at a global level. This was achieved by registering each subject's structural data to

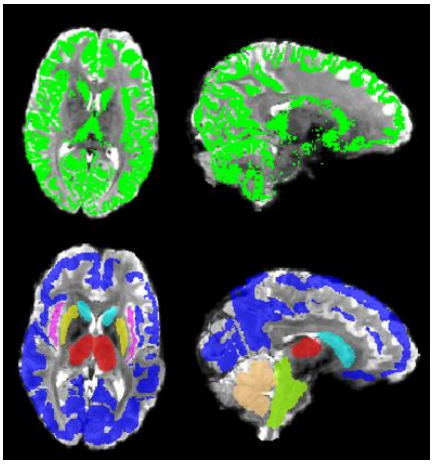

Figure 2 – ROIs defined in the one subject's functional space: segmented gray matter (light green), cortical gray matter (dark blue), thalamus (red), caudate nucleus (light blue), putamen (yellow), insula (purple), cerebellum (brown) and brainstem (dark green).

MNI, followed by segmentation. The GM partial volume estimate map was threshold at 0.7 (threshold was chosen to be less stringent to avoid inadvertently removing important functional regions of GM tissue) and registered to the functional space. To differentiate cortical gray matter from other brain structures, masks of the four brain lobes, as well as the caudate nucleus, cerebellum, insula, putamen and thalamus were extracted from the MNI structural atlas. All masks were registered to functional space (the four lobes were added together to obtain a cortical gray matter mask) by non-linear registration. A brainstem mask, taken from the Harvard-Oxford subcortical structural atlas, was also registered to the functional space.

3. Results and Discussion

3.1. Extended RETROICOR model

The results of the Fourier order optimization methodology based on Harvey et al. 2008 are summarized in Table 1.

Regressor Set	Test	Regressor Set	Test
1C	1C	Drifts	**1.400**
1R	1R	Drifts	**1.296**
2C	2C1R	1C1R	**0.142**
2R	1C2R	1C1R	**0.332**
3C	3C2R	2C2R	**0.125**
3R	2C3R	2C2R	0.066
4C	4C3R	3C3R	0.062
4R	3C4R	3C3R	0.084
1X	3C2R1X	3C2R	-0.004
21X	3C2R21X	3C2R	0.070
12X	3C2R12X	3C2R	0.063
22X	3C2R22X	3C2R	0.151
1C,2C, 1R,2R	2C2R	Drifts	**3.171**
1C,2C,3C, 1R, 2R	3C2R	Drifts	**3.268**

Table 1 – Average VE by each extended RETROICOR order in gray matter (average results). The last two rows show the VE by the original RETROICOR proposition (2 Fourier orders) and the deemed optimal model. Interaction components (X) are preceded by two numbers: the first identifies the cardiac order, while the second identifies the respiratory order. The values in bold show the group means that are above a threshold defined by a one-sided paired t-test performed at a significance level of 0.05. The last two rows show the VE by the original and extended RETROICOR models.

The first (fundamental) Fourier order of both cardiac and respiratory components explains the most variance in the model with a combined group average of 2.7 ± 0.1 %. VE by each consecutive order evolves in a descending trend with the exception of the difference between the 3rd and 4th respiratory orders (this inversion in the trend, however, is not significant as neither VE_{3R} or VE_{3R} were deemed statistically significant). The original RETROICOR model, which comprises the first two Fourier orders, was found to explain an average 3.2 ± 0.1 % of the fluctuations in the GM. A significant effect was also found for the 3rd cardiac order, however no further respiratory orders or interaction effects were found to be significant. The optimal model, 3C2R, improves only marginally when compared to the original proposition, explaining 3.3 ± 0.1 % of the variance in GM.

In the original paper by Harvey, a more complex model (3C4R11X using the same nomenclature) was deemed optimal. Results coincide when cardiac effects are considered, however effects resulting from higher respiratory harmonics as well a low order interaction between cardiac and respiratory cycles were also found to be significant in this study. There are, however, two key differences between the methodology followed by Harvey and the one presented here.

Firstly, Harvey study focused specifically on brainstem (however, a broader ROI was defined, including other subcortical structures, vascular regions, the thalamus and ventricles), rather than a global gray matter effect. While the respiratory effect does not seem to be particularly prominent in brainstem itself, the VE maps show an important respiratory correlation in ventricles and CSF filled subcortical regions, which are excluded from the average results in this work but are not in Harvey's. Inclusion of these highly respiratory modulated regions is expected to considerably increase the respiratory contribution and motivate the inclusion of higher respiratory harmonics. In order to make the results more directly comparable to Harvey's, VE for every set of regressors was averaged over the previously defined brainstem mask (it should be noted, however, that the brainstem mask defined in this study is considerably more specific, excluding, for example, pure CSF and large vascular regions). Interaction effects were found to be significant ($p>0.02$) up to the 2nd order. Higher contributions in lower brain regions are a consequence of the intrinsic physiological nature of these interactions: as observed by Brooks et al. (2013), increased cardiac output through the respiratory pump mechanism (Linn et al., 1999) is likely to be an important source of confound in data of the brainstem due to its proximity to large vessels. In fact, the introduction of interaction terms was originally motivated by a physiological noise modelling study in spinal cord (Brooks et al., 2008), in which interaction mechanisms were found to explain a significant fraction of the signal. These were later confirmed in subsequent publications directed at the same imaged region (Kong et al., 2012) and extended to the brainstem, as is the case of Harvey's work. No reports on these effects in other brain regions were found in the literature. The results presented in this work, however, suggest that interaction effects are not a major source of concern in cortical regions.

Secondly, Harvey used a binomial threshold to calculate the number of significant F-test voxels required to include a particular set of regressors in the model, rather than assessing the significance of the mean effect. This approach guarantees that a regressor is only included in the model when a significant number of voxels in the tested ROI benefits from its inclusion. While arguably more representative of the evaluated ROI, it does not account for spatial focused effects, which, despite affecting a restricted area, may be highly significant and introduce spurious correlations when testing for connectivity.

No studies are known to have carried out a systematic ROI-based analysis on VE by physiological sources of confound. Hence, direct comparison for specific brain regions is not possible. However, in Bianciardi et al. (2008) and Jorge J. et al. (2013), sources of signal fluctuation are evaluated at a global level (across GM) in data at 7T by means of a nested model approach in which this work was based. These studies report an individual RETROICOR (using the original 2 order model) VE of respectively 2.6 ± 0.8 % and 5.0 ± 0.8 % in gray matter. While the former is in agreement with the findings in this work, being only slightly lower, the latter points to a noticeably increased effect of the RETROICOR component. This significant difference is most likely due to

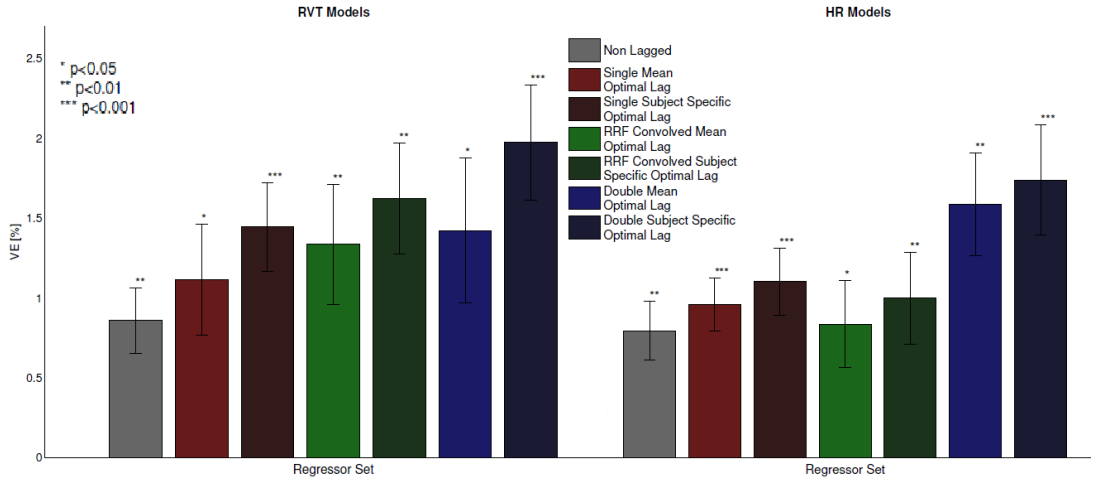

Figure 3 – Average variance explained by each tested RVT and HR model in GM.

method used to define the GM mask: in Jorge J. et al., 2013, the correlation between each voxel time course and the mean brain time course was computed and the voxels with the 10% highest correlation (after exclusion of negatively correlated voxels) are selected to integrate the GM mask. As discussed in the same paper, while generally accurate, this method is also vulnerable to the inclusion of large blood vessels such as the sagittal sinus. Vascular regions are highly modulated by cardiac and respiratory periodic phenomena and, thus, they are likely to display an increased RETROICOR contribution when compared to legitimate GM tissue, as the findings by Jorge J. suggest.

3.2. RVT and HR model optimization

The results obtained from the set of 14 RVT and HR models tested is shown in Fig. 3. The analysis of variance reported no significant differences on the mean VE by RVT and HR. A significant main effect, however, was found for both type of model used ($p=0.002$) and lag specificity ($p=0.01$). No interaction effects were found to be significant. The post-hoc analysis performed on the analysis of variance showed that the subject specific double-lag approach significantly explains the most variance in the data in both RVT ($p>0.023$, Bonferroni corrected) and HR ($p>0.016$, Bonferroni corrected) cases. Convolving with either RRF or CRF was not found to explain significantly more variance when compared to using a single-peak. The post-hoc analysis also revealed that opting for a double-lag approach over convolving RVT with RRF is only significant ($p=0.023$) when each subject's peaks are considered, as no significant differences between the two approaches were found when peaks were extracted from the group average.

When evaluated over the the previously defined ROIs, the average VE by the optimized subject specific double-lag model was similar for RVT and HR, as no significant differences between the two were found within each ROI. HR was found to explain the most variance (2.0 ± 0.4 %) on the insular cortex and the least on the cerebellum (1.0 ± 0.2 %). The most VE by RVT was measured on cortical gray matter regions (2.1 ± 0.4 %), while the least was measure on the putamen (0.9 ± 0.2 %). Inspection of the RVT VE maps reveals that these cortical regions are mainly located in the occipital lobe (Fig. 4, Left). HR maps show a more heterogenous distribution from subject to subject, however an increased contribution in the frontal lobe and localized clusters in occipital and insular cortex are consistently observed across subjects (Fig. 4, Right).

Bianciardi et al. (2008) and Jorge J. et al., (2013) report a VE of respectively 2.6 ± 0.8 % and 2.46 ± 0.90 % for RVT and 1.7 ± 0.6 % and 3.50 ± 1.03 % for HR, averaged over GM. Similarly to what was observed in 3.1, Jorge J. et al.'s VE estimates are considerably higher than the ones found in this study (1.9 ± 0.3 % for RVT and 1.7 ± 0.3 % for HR, averaged over GM). Again, these differences are most likely related to the different approaches used to define the GM ROI. Due to the cardiac and respiratory origins of HR and RVT, inclusion of vascular regions is likely to result in overestimation of their contributions. The VE spatial distribution shown in Fig. 4 add to these considerations as both RVT and HR maps, in fact, show higher contributions close to the sigmoid sinus and the region of sinus

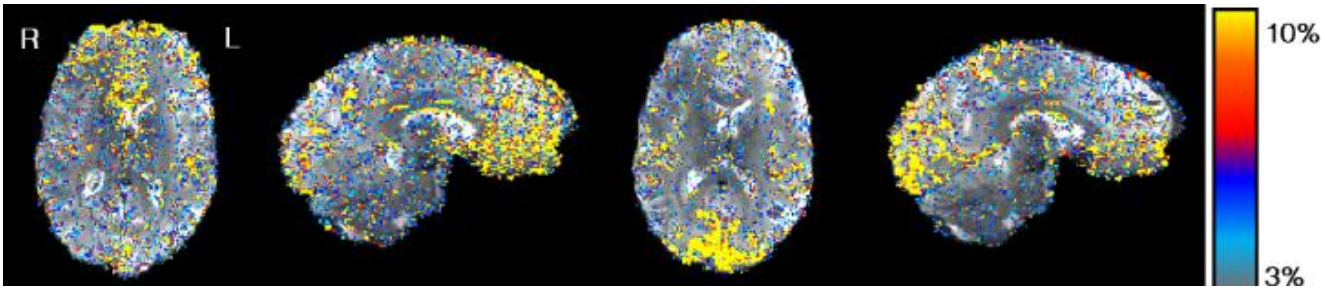

Figure 4 – Representative axial and sagittal slices taken from one subject's RVT and HR variance explained maps; (Left) The sagittal cut shows a widespread HR effect in the frontal lobe with smaller, more focused, regions of the occipital and temporal lobes also being notoriously affected, as evidenced by the axial cut; (Right) Signal fluctuations in the occipital lobe appear to be highly affected by RVT effects, particularly in the regions close to the transversal sinus (axial cut); smaller regions in the temporal and lower sections of the frontal lobes are also shown to be susceptible to RVT effects (sagittal cut).

confluence, which, if considered when averaging over GM, will result in increased VE estimations.

When compared to Bianciardi results, a very close match is found for HR, however RVT contributions to variance were found to be higher than in the present work. A possible explanation might be related to the difference on how RVT was extracted in both works. In Bianciardi study, a cumulative integral (C) of the respiratory signal was computed and the value of RVT at instant t was taken as the difference between C at t+TR/2 and t-TR/2. This method was based on the method developed by Birn et al. (2008), however it is slightly less computationally demanding (Bianciardi et al., 2009). Despite the obvious differences between this method and the one based on Chang et al. (2009) followed in the present work, it is unclear whether it should translate into an overestimation or underestimation of the VE and, thus, it does not fully answer our question. Another important difference has to do with the intermediate spurious time points removal step performed here. While this step was intended to improve the regressor performance, it might have had the opposite effect by making it too conservative. Further investigation of this topic would require a thorough connectivity study on the RVT corrected and uncorrected data using both RVT propositions, which is out of the scope of this study.

3.3. CSF and WM average time courses

A side by side comparison of the CSF masks and time courses extracted from them for a representative subject is presented in Fig. 5.

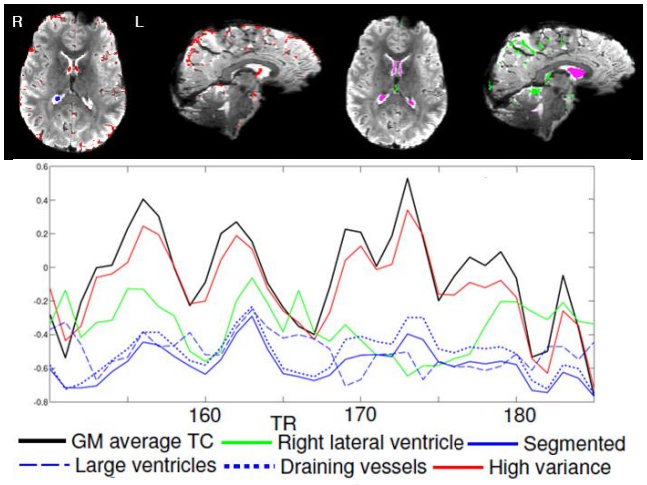

Figure 5 – Side by side comparison of the CSF masks and extracted CSF time courses for one representative subject; (Top) Axial and sagittal cuts of the high variance mask (red), right lateral ventricle mask (blue), large ventricles mask (purple) and draining vessels mask (green) are depicted (the segmented CSF mask is obtained from the concatenation of the draining vessels and large ventricles masks); (Bottom) Section of the extracted CSF time courses, overlaid with the average GM time course for ease of comparison.

CSF time courses extracted from the high variance mask, as well as from the segmented and draining vessels masks, who all include peripheral CSF regions, show striking similarities with the average GM time course (the most noticeable similarities being observed between the GM TC and $X_{HV\ CSF}$). It is important to note that the average GM time course analyzed here was obtained from a very stringent GM mask (the GM partial volume estimate was thresholded at 0.98) and, thus, CSF contamination of the GM time course itself, while possible, is very unlikely. Another interesting observation is that peripheral CSF seems to dominate most of the CSF fluctuations as the segmented and draining vessels time courses are very similar. These results were confirmed by computing the correlations between all the considered CSF regressors and the GM average TC (Fig. 6). All masks including CSF regions outside of the ventricles are shown to be highly correlated with the GM time course. What is less obvious is the higher correlation found between the GM time course and $X_{RLV\ CSF}$ when compared to the correlation between GM and $X_{LV\ CSF}$. Since the right lateral ventricle mask is arguably more conservative, one would expect this

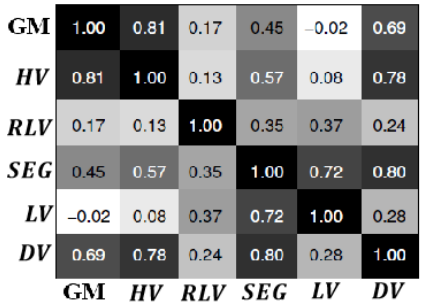

Figure 6 – Correlation matrix averaged over all subjects, showing the correlations between all CSF regressors with the GM average time course added as a reference. The highest collinearity is found between the GM time course and $X_{HV\ CSF}$ (0.81), followed by $X_{DV\ CSF}$ (0.69) and $X_{SEG\ CSF}$ (0.45). The lowest collinearity is found between the GM time course and $X_{LV\ CSF}$ (-0.02), followed by $X_{RLV\ CSF}$ (0.17). The highest collinearity between CSF masks is found between $X_{SEG\ CSF}$ and $X_{DV\ CSF}$ (0.80) while the lowest is found between $X_{HV\ CSF}$ and $X_{DV\ CSF}$ (0.08).

time course to be the least correlated with the average GM signal. A plausible explanation is the error introduced by minor defects when registering from the standard space to the functional space. Visual inspection revealed that errors in registration, in fact, occur, which, given the reduced size of the mask, may introduce non negligible GM signal fluctuations in the average signal extracted. While this is certainly a problem also shared by the large ventricles mask, the fact that an average of 4 ventricles time courses is taken mitigates this effect.

Extracting an accurate WM average time course poses much of the same challenges and, thus, a similar approach was carried out. Before erosion, the average WM time course shows obvious similarities with the GM average time course. The erosion step dramatically reduces the collinearity between the two time courses in the majority of the subjects, yielding what is arguably a better representation of global WM fluctuations (Fig. 7).

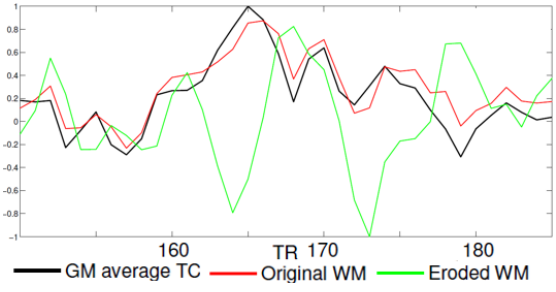

Figure 7 – Section of the WM time courses extracted from the regular and eroded WM masks, overlaid with the average GM time course for ease of comparison, showing the effect of the erosion step on the average WM time course.

The results presented in this section clearly show that the confound regressors extracted from the fMRI data are highly sensitive to the method used to define their representative regions. CSF time courses extracted from less specific maps (high variance and draining vessels) are shown to significantly explain additional variance in the data ($VE_{GM}(X_{HV\ CSF}) = 2.8 \pm 0.6\ \%$; $VE_{GM}(X_{DV\ CSF}) = 2.1 \pm 0.4\ \%$) which was not accounted for by the model based only on external physiological acquisitions. However, the high correlation found between these and the average GM time course suggest that a substantial portion of the signal of interest will be lost if these contributions are regressed out of the data. By analyzing the spatial pattern of the DMN, Jo Hang et al. (2010) reported similar results when regressing out $X_{LV\ CSF}$ alone and both $X_{LV\ CSF}$ and $X_{DV\ CSF}$. However, the characteristic bilateral patterns of the DMN were clearer when only $X_{LV\ CSF}$ was regressed out. Hence, the optimal model suggested by Jo Hang featured only a CSF average time correction based on intra-ventricular fluctuations. While the presence of this effect cannot be confirmed in the data analyzed here as functional connectivity was not assessed, both collinearity with the GM time course and the drastic VE reduction in GM tissue when increasing the CSF map specificity are strong indicators that partial volume effects with GM (and not true predictive power of confounding fluctuations in the GM) are in the origin of the apparently good performance of less specificity CSF regressors. As a consequence of these findings, both high variance and draining vessels CSF average time courses will be disregarded in future models. If, however, a very specific functional response is sought and the consequences of partially leaving out signal of interest is not a major concern, regressing out these regressors might be considered. In that case, assuming that a reasonable segmentation of the brain is obtained, $X_{DV\ CSF}$ is preferable to $X_{HV\ CSF}$ as it does not make assumptions on the relation between signal's variability and physiological source.

When partial volume effects were kept to a minimum, much lower average VE values were obtained ($VE_{GM}(X_{RLV\ CSF}) = 0.5 \pm 0.2\ \%$, $VE_{GM}(X_{LV\ CSF}) = 0.6 \pm 0.1\ \%$). Although no significant ($p>0.05$) difference was found between $VE(X_{RLV\ CSF})$ and $VE(X_{LV\ CSF})$ in GM, $X_{LV\ CSF}$ was considered to best model CSF spurious fluctuations due to the following reasons: $X_{CSF\ LV}$ better represents the group effect (SE is one order of magnitude lower); collinearity with the GM time course measured through PCC was found to be lower; $X_{LV\ CSF}$ is less susceptible to registration errors, increasing the confidence that no PVE bias is introduced in VE estimates. Hence, $X_{LV\ CSF}$ is employed in future comparisons.

3.4. Motion induced confounds

Due to the high inter-subject variability, VE results in GM are shown for the entire sample (Fig. 8).

	S1	S2	S3	S4	S5	S6	S7	S8	S9	Avg.	SE
MCFLIRT estimates	2.495	4.478	3.232	7.298	9.355	6.686	5.009	2.003	4.703	**5.030**	**0.798**
DVARS-FD spikes	0.890	0.008	3.512	-	2.107	0.064	0.093	0.080	0.422	**0.897**	**0.450**
# DVARS spikes	18	7	26	2	17	6	4	2	2	**9**	**3**
# FD spikes	15	6	15	9	17	11	8	10	7	**11**	1
# Dual-criteria spikes	9	1	12	0	8	2	1	1	2	**4**	**1**

Figure 8 – Subject to subject and group results for the VE explained, number of motion spikes identified by DVARS and FD and the number of peaks simultaneously identified by both criteria.

Subtle motion artefacts rather than abrupt, large, motion are shown to have a much larger contribution both at a global ($VE_{GM}(X_{MCFLIRT}) = 5.0 \pm 0.8, VE_{GM}(X_{DVARS-FD}) = 0.9 \pm 0.5$) and spatially specific (the lowest $VE(X_{MCFLIRT})/VE(X_{DVARS-FD})$ ratio (3.24) is observed in the brainstem where $VE_{brainsetm}(X_{MCFLIRT}) = 3.0 \pm 0.8, VE_{brainstem}(X_{DVARS-FD}) = 0.9 \pm 0.5$). This is in line with the reports by Power et al., 2010 and Satterthwaite et al., 2013: while no information regarding VE is explicitly stated for the components, both studies report a considerably more important impact from subtle motion (<0.5 mm), with spurious short range and right-left connections, as well as reduced long-range and anterior-posterior connectivity being associated with the effects of subtle voxel displacement.

3.5. A closer look on data-based and physiological acquisitions derived confounds shared variance

There might be scenarios where acquisition of external recordings is not possible or is unavailable. Is such situations, modelling of physiological noise becomes restricted to data-based corrections. Thus, how well can one expect to regress out physiological contributions solely using information in the fMRI data becomes a relevant question. To answer this question, the fraction of shared variance between the regressor set derived from external measurements and the regressor set consisting of the CSF and WM time courses was computed. In this context, regressing out a less conservative CSF time-course at the cost of some signal loss might be required to reduce residual nuisance in the data to an acceptable level. Thus, shared variance was measured for two different sets, one which is very specific, $X_{LV\ CSF} + X_{WM\ erod}$ and another which is less conservative, however with a considerable probability of also removing signal of interest, $X_{LV\ CSF} + X_{DV\ CSF} + X_{WM\ erod}$.

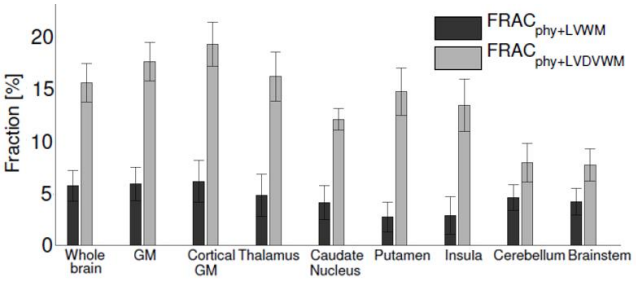

Figure 9 – Fraction of the variance explained by the set of regressors obtained from external physiological acquisitions that can be alternatively be explained by average confound regressors extracted directly from the fMRI data.

The degree of shared variance between $X_{LV\ CSF}$ is generally low, with the maximum fraction being reported in cortical gray matter ($FRAC_{LVWM} = 6.1 \pm 2.0\ \%$). Shared variance is noticeably higher when comparing shared variance between the set $[X_{LV\ CSF}\ X_{DV\ CSF}]$ and X_{phy}, with the maximum fraction also being reported in cortical gray matter ($FRAC_{SEGWM} = 19.3 \pm 2.1\ \%$). Significant differences are found between $FRAC_{LVWM}$ and $FRAC_{LVDVWM}$ at $p>0.001$ in all regions, except for the cerebellum and brainstem, where the differences are still significant but at $p>0.05$. These results show that, if a less conservative approach is used to model CSF, one can expect to model approximately 19% of the VE by the set of regressors extracted from external physiological acquisitions in GM. If $X_{LV\ CSF}$ alone is used to model CSF, then only 6% of the VE by cardiac/respiratory effects is expected to be regressed out. These results show that an important portion

of the confounds removed by regressing out respiratory and cardiac effects will still be present in the data if only data-based methods are used. Additionally, by alternatively modelling these effects using a less conservative set of CSF regressors, some signal of interest is expected to be lost. As a final consequence, the results presented in this section strongly suggest that data-based methods alone are not a suitable alternative to modelling cardiac and respiratory mechanisms through external acquisitions.

3.6. The final model

The individual analysis carried out for each noise component resulted in an optimal model consisting of 25 regressors, plus a variable number (ranging from 0 to 12) of regressors depending on the number of volumes affected by large motion in each subject. A summary of the group results found throughout this work, featuring the VE in different brain regions by each set of regressors included in the optimal model, is shown in Fig. 10.

The final model is shown to explain a total of 33.8 ± 5.8 % variance (either low-frequency drifts, cardiac/respiratory effects, data fluctuations or motion), WM and CSF global fluctuations are reported to explain the least variance in the signal both at a GM level (1.4 ± 0.2 %) and at the brain regions specified (the maximum value is reported at the caudate nucleus, 1.7 ± 0.3 %). CSF/WM fluctuations (1.4 ± 0.2%), motion (6.0 ± 1.2 %), cardiac/respiratory (6.6 ± 1.2 %) effects and slow drifts (19.6± 3.3 %) in the data successively explain more variance in GM, with same tendency being observed across all considered ROIs.

Similar contributions from cardiac and respiratory signal are observed in Bianciardi's work (7.9%), while slightly higher values are found in Jorge J.'s work (10.8%). Contributions from low-frequency signals are reported to be higher in both publications (35.3% and 27.9% in Bianciardi and Jorge J., respectively). Global CSF and WM fluctuations in the data and motion artefacts were not quantified in these studies. In Biaciardi's study, the thermal noise was estimated by means of an additional acquisition where no RF excitation was applied with the aim of measuring its relative contribution in the data only, as no modelling of this component was performed. Some differences in results can be objectively attributed to the

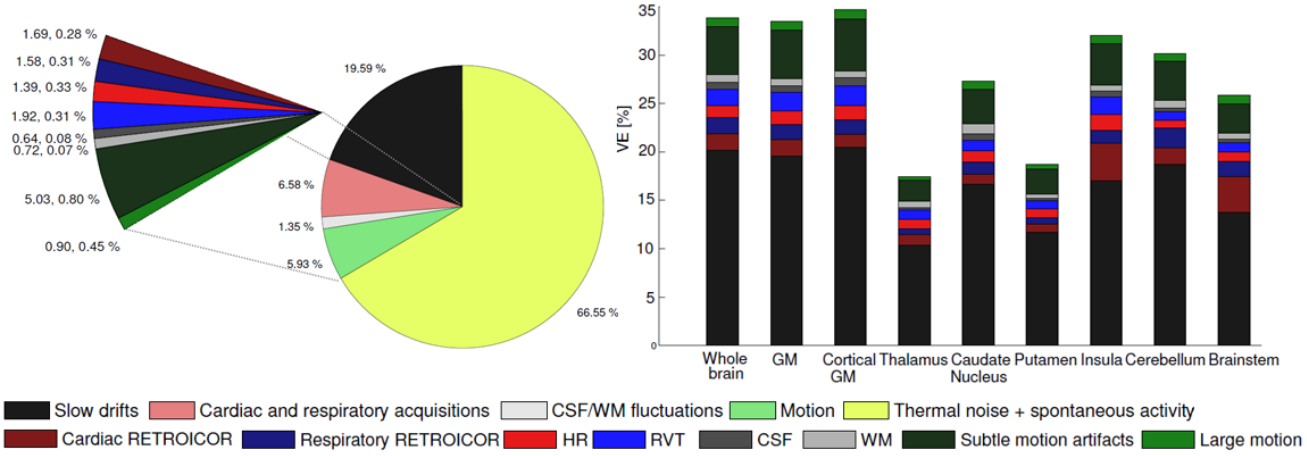

Figure 10 – Variance explained by the optimal model; (Left) Regressors contributing to the variance explained in GM are subdivided in two levels: the broader tier arranges the regressors in groups that reflect their physiological source, while the more descriptive tier organizes the regressors sets by model/confound; (Right) Variance explained by each set of regressors in the previously defined ROIs.

putatively attributable to nuisance sources in gray matter: 19.6% of the signal variance in GM is explained by low-frequency drifts; 13.9% is attributed to motion, cardiac and respiratory mechanisms, as well as fluctuations at a global level in CSF and WM tissues; the remaining 66.6% are attributed to neuronal spontaneous activity and thermal noise. While the performance of the model is very similar in certain regions, some important differences are observed in others (a one-way analyses of variance on the ROI effect yielded a 3.36 F-score, p=0.0025). When averaging results over the whole brain or restringing them to cortical gray matter, no significant differences are observed when compared to GM averages, with 33.8% (13.7% of variance attributable to effects other than low-frequency drifts) and 34.7% (14.2% of variance attributable to effects other than low-frequency drifts) being explained by the model. The model explained the least variance in the thalamus (17.4%) and putamen (18.71%), with both average VEs being significantly lower than the average computed for the whole brain (p>0.0001). As previously shown, cardiac effects (these include the cardiac RETROICOR component and heart rate) are particularly accentuated in the insular cortex and in the brainstem, with a variance of 5.5% and 4.6% being respectively explained in these regions (the whole brain average is 2.9%, deemed significantly different at p>0.0001). When considering the physiological source of the regressors

methods used for GM ROI definition and regressors extraction techniques (in particular, regarding RVT). However, other less objectively quantifible effects make it difficut to draw accurate comparisons. Despite the effort to ensure that a direct comparison is possible between the present work and similar publications, a number of variable factors affect the estimation of nuisance contribuitions and therfore, hinder the reliability of a direct comparison. As shown by Triantafyllou et al., 2005, 2011, even when imaging at the same field strength, important differences are observed in the physiological to thermal noise ratio when certain acqisition parameters. In particular, Triantafyllou found an increase in the physiological to thermal noise from 0.91 ± 0.13 to 1.54 ± 0.14 when increasing voxel size from 1 X 1 X to 2 X 2 X 3 mm^3. These findings are in line with the tendency verified in this work, as the physiological contributions are generally higher in Jorge et al. 2013 (where the voxel size – 2 mm^3 isotropic – used is highest) and lower in this work (where the voxel size – 1.1 mm^3 isotropic – is lowest). In addition to acquisition parameters, different pre-processing steps (in particular, the order at which certain steps such as temporal filtering, slice timing and motion correction are performed and the amount of spatial of smoothing applied to the data) may potential lead to differences in physiological noise estimations. No systematic description of these effects was found in the literature, however Carp et al., 2013 reports important

differences in estimation of motion artefacts when performing time filtering at different times in the pre-processing pipeline. Hence, when evaluating the results presented in this work, it is important to keep in mind that physiological modeling is highly dependent on a wide range of factors and some care is required when drawing comparisons with studies performed under different conditions.

A systematic study on the VE by different sources of physiological noise at different brain regions is not found in the literature which invalidates a direct comparison with similar studies. However, modeling of physiological noise in the brainstem, in particular, has recently received more attention in both resting-state and task activation fMRI studies (Harvey et al., 2008; Brooks et al., 2013; Beissner et al., 2014) due to the extra difficulties associated with imaging in this region. The results obtained in the present study, in fact, show the 2nd highest contribution of cardiac and respiratory mechanisms (8.2 ± 1.4 %, only surpassed by the insular cortex, with 9.8 ± 1.7 %), however the overall performance of the model is poorer when compared to other regions as the source of 74.1 % of the signal variance is still unknown after accounting for physiological sources. A substantial loss of performance has to do with the decrease of VE by the drifts set, suggesting that fast oscillations not accounted by current modelling techniques, rather than low-frequency fluctuations, are responsible for a substantial part of the signal variation in the brainstem. In Brooks et al., 2013, a correction method using a GLM framework (the composition of the model is not specified) was used to correct images at 3T (3 mm^3) and 7T (1 mm^3 and 2 mm^3), with results being reported in terms of temporal SNR. Brooks' findings show that correcting for physiological noise through a GLM approach yields significantly improved results in the cortex (increases in 100% are frequently observed across all field strength and resolutions), while only modest improvements are reported in the brainstem (an average of 12.5%). Despite not directly measuring physiological contributions by explicitly computing their VE, the generally low increases in tSNR shows that currents methods are still not able to adequately model an important fraction of the signal variation in the brainstem.

4. Conclusions

The results obtained and the considerations made throughout this study showed that, in fact, physiological noise represents a substantial fraction of signal variance when imaging at high field strength. By using a combination of well-established and promising state-of-the-art techniques, a very representative fraction of spurious variation in the signal could be identified and regressed out. Increased cardiac and respiratory related artefacts were found in intrinsically high noise regions such as the brainstem and the cerebellum, however an important portion of signal variance in these regions could still not be adequately modelled by current techniques. The original RETROICOR proposition presented significant results when modeling quasi-periodic cardiac and respiratory effects at a global level. While marginal improvements were obtained when using higher order cardiac harmonics, interaction effects did not pose a major concern when assessing performance in gray matter as a whole. Accounting for these when imaging particular subcortical structures, however, was shown to be valuable. When modelling non-periodic, low frequency, cardiac and respiratory signals, a double-lag approach at a subject level was found to be the most effective. While the overall shape of the hemodynamic response is well described by the impulse responses proposed in the literature, the high inter-subject variability regarding onset and peak-to-peak timings suggested that a standardized response may not be suitable. As a result of the conservative approach followed to avoid loss of signal of interest, global fluctuations in white matter and CSF improved only slightly to the model. Subtle voxel displacements, rather than large, abrupt, motion were found to be the most problematic. An additional analysis revealed that external physiological acquisitions are invaluable when modelling cardiac and respiratory confounds as data-based techniques are unable to model an important fraction of the spurious variance introduced by these effects.

In summary, having the mind that different acquisition and processing pipelines do not allow the prescription of an universally optimal physiological model, the quantitative characterization and guidelines provided in this work are thought to be an important contribution to the understating and improvement of physiological modelling techniques in data at high field strengths. Future work includes the extraction of slice-specific regressors (rather than volume-specific), performing a connectivity study on the corrected data to evaluate improvements in recognition of spatial patterns and comparison of the results found with automated ICA methods to identify and eliminate nuisance signal components.

Acknowledgements

A note of gratitude goes to Prof. Patrícia Figueiredo, who supervised this work, to Marta Bianciardi and Lawrence Wald from the Athinoula A. Martinos Center for Biomedical Imaging who acquired and provided the data for this study, and to Juliana Rodrigues, Rodolfo Abreu and Afonso Dias, who worked on the pre-processing and registration steps of the pipeline.

REFERENCES

Beckmann, Christian F., and Stephen M. Smith. "Probabilistic independent component analysis for functional magnetic resonance imaging." Medical Imaging, IEEE Transactions on 23.2 (2004): 137-152.

Beissner, Florian, and Simon Baudrexel. "Investigating the human brainstem with structural and functional MRI." Frontiers in human neuroscience 8 (2014).

Bianciardi, Marta, et al. "Sources of functional magnetic resonance imaging signal fluctuations in the human brain at rest: a 7 T study." Magnetic resonance imaging 27.8 (2009): 1019-1029.

Birn, Rasmus M., et al. "Separating respiratory-variation-related fluctuations from neuronal-activity-related fluctuations in fMRI." Neuroimage 31.4 (2006): 1536-1548.

Birn, Rasmus M., et al. "The respiration response function: the temporal dynamics of fMRI signal fluctuations related to changes in respiration."Neuroimage 40.2 (2008): 644-654.

Birn, Rasmus M. "The role of physiological noise in resting-state functional connectivity." Neuroimage 62.2 (2012): 864-870.Fachinger, J., den Exter, M., Grambow, B., Holgerson, S., Landesmann, C., Titov, M., et al. (2004).

Brooks, Jonathan CW, et al. "Physiological noise in brainstem fMRI." Frontiers in human neuroscience 7 (2013).

Carp, Joshua. "Optimizing the order of operations for movement scrubbing: Comment on Power et al." Neuroimage 76 (2013): 436-438.

Chang, Catie, John P. Cunningham, and Gary H. Glover. "Influence of heart rate on the BOLD signal: the cardiac response function." Neuroimage 44.3 (2009a): 857-869.

Chang, Catie, John P. Cunningham, and Gary H. Glover. "Influence of heart rate on the BOLD signal: the cardiac response function." Neuroimage 44.3 (2009a): 857-869.

Chang, Catie, and Gary H. Glover. "Effects of model-based physiological noise correction on default mode network anti-correlations and correlations."Neuroimage 47.4 (2009c): 1448-1459.

Churchill, Nathan W., et al. "PHYCAA: data-driven measurement and removal of physiological noise in BOLD fMRI." Neuroimage 59.2 (2012): 1299-1314.

de Zwart, Jacco A., et al. "Reducing correlated noise in fMRI data." Magnetic Resonance in Medicine 59.4 (2008): 939-945.

Glover, Gary H., Tie-Qiang Li, and David Ress. "Image-based method for retrospective correction of physiological motion effects in fMRI: RETROICOR."Magnetic Resonance in Medicine 44.1 (2000): 162-167.

Greitz, D., A. Franck, and B. Nordell. "On the pulsatile nature of intracranial and spinal CSF-circulation demonstrated by MR imaging." Acta radiologica 34.4 (1993): 321-328.

Harvey, Ann K., et al. "Brainstem functional magnetic resonance imaging: disentangling signal from physiological noise." Journal of Magnetic Resonance Imaging 28.6 (2008): 1337-1344.

Hu, Xiaoping, et al. "Retrospective estimation and correction of physiological fluctuation in functional MRI." Magnetic resonance in medicine 34.2 (1995): 201-212.

Jenkinson, Mark, et al. "Improved optimization for the robust and accurate linear registration and motion correction of brain images." Neuroimage 17.2 (2002): 825-841.

Jenkinson, Mark, et al. "Fsl." Neuroimage 62.2 (2012): 782-790.

Jo, Hang Joon, et al. "Mapping sources of correlation in resting-state FMRI, with artefact detection and removal." Neuroimage 52.2 (2010): 571-582.

Jorge, João, et al. "Signal fluctuations in fMRI data acquired with 2D-EPI and 3D-EPI at 7 Tesla." Magnetic resonance imaging 31.2 (2013): 212-220.

Kong, Yazhuo, et al. "Assessment of physiological noise modelling methods for functional imaging of the spinal cord." Neuroimage 60.2 (2012): 1538-1549.

Krüger, Gunnar, and Gary H. Glover. "Physiological noise in oxygenation-sensitive magnetic resonance imaging." Magnetic Resonance in Medicine 46.4 (2001): 631-637.

Lin, T. Physiology of the circulation" in Fundamentals of Anaesthesia, eds C. Pinnock, T .Lin, and T. Smith, London: Greenwich Medical Media (1999) 331–360.

Malinen, Sanna, et al. "Improved differentiation of tactile activations in human secondary somatosensory cortex and thalamus using cardiac-triggered fMRI."Experimental brain research 174.2 (2006): 297-303.

Muresan, Lucian, et al. "Automated correction of spin-history related motion artefacts in fMRI: simulated and phantom data." Biomedical Engineering, IEEE Transactions on 52.8 (2005): 1450-1460.Dagli, Mandeep S., John E. Ingeholm, and James V. Haxby. "Localization of cardiac-induced signal change in fMRI." Neuroimage 9.4 (1999): 407-415.

Pfeuffer, Josef, et al. "Correction of physiologically induced global off-resonance effects in dynamic echo-planar and spiral functional imaging." Magnetic Resonance in Medicine 47.2 (2002): 344-353.

Power, Jonathan D., et al. "Spurious but systematic correlations in functional connectivity MRI networks arise from subject motion." Neuroimage 59.3 (2012): 2142-2154.

Purdon, Patrick L., and Robert M. Weisskoff. "Effect of temporal autocorrelation due to physiological noise and stimulus paradigm on voxel-level false-positive rates in fMRI." Human brain mapping 6.4 (1998): 239-249.

Raj 2001 - Raj, Devesh, Adam W. Anderson, and John C. Gore. "Respiratory effects in human functional magnetic resonance imaging due to bulk susceptibility changes." Physics in medicine and biology 46.12 (2001): 3331.

Satterthwaite, Theodore D., et al. "An improved framework for confound regression and filtering for control of motion artefact in the preprocessing of resting-state functional connectivity data." Neuroimage 64 (2013): 240-256.

Smith, Stephen M., et al. "Advances in functional and structural MR image analysis and implementation as FSL." Neuroimage 23 (2004): S208-S219.

Smith, Stephen M., et al. "Resting-state fMRI in the human connectome project." Neuroimage 80 (2013): 144-168.

Triantafyllou, C., et al. "Comparison of physiological noise at 1.5 T, 3 T and 7 T and optimization of fMRI acquisition parameters." Neuroimage 26.1 (2005): 243-250.

Triantafyllou, Christina, Jonathan R. Polimeni, and Lawrence L. Wald. "Physiological noise and signal-to-noise ratio in fMRI with multi-channel array coils." Neuroimage 55.2 (2011): 597-606.

Wald, Lawrence L. "The future of acquisition speed, coverage, sensitivity, and resolution." NeuroImage 62.2 (2012): 1221-1229.

Weissenbacher, Andreas, et al. "Correlations and anticorrelations in resting-state functional connectivity MRI: a quantitative comparison of preprocessing strategies." Neuroimage 47.4 (2009): 1408-1416.

Wise, Richard G., et al. "Resting fluctuations in arterial carbon dioxide induce significant low frequency variations in BOLD signal." Neuroimage 21.4 (2004): 1652-1664.